ASIAN JOURNAL OF FORESTRY
Volume 9, Number 2, December 2025
Pages: 166-181

E-ISSN: 2580-2844
DOI: 10.13057/asianjfor/r090202

Estimating mangrove above-ground biomass using GEDI LiDAR, Sentinel data, and machine learning in Rawa Aopa National Park, Indonesia

ZULKARNAIN[1,♥], M. BUCE SALEH[2], HERI PURNOMO[2], BUDI KUNCAHYO[2], TATANG TIRYANA[2], NINING PUSPANINGSIH[2]

[1]Program of Forest Management Science, Graduate School, Institut Pertanian Bogor. Jl. Raya Dramaga, Kampus IPB Dramaga, Bogor 16680, West Java, Indonesia. Tel.: +62-251-8621677, Fax.: +62-251-8621256, ♥email: zulkarnain@uho.ac.id

[2]Department of Forest Management, Faculty of Forestry and Environment, Institut Pertanian Bogor. Jl. Raya Dramaga, Kampus IPB Dramaga, Bogor 16680, West Java, Indonesia

Manuscript received: 22 May 2025. Revision accepted: 3 August 2025.

Abstract. *Zulkarnain, Saleh MB, Purnomo H, Kuncahyo B, Tiryana T, Puspaningsih N. 2025. Estimating mangrove above-ground biomass using GEDI LiDAR, Sentinel data, and machine learning in Rawa Aopa National Park, Indonesia. Asian J For 9: 166-181.* Accurate above-ground biomass estimation is crucial for climate change mitigation and sustainable mangrove management. Therefore, this study aimed to integrate Global Ecosystem Dynamics Investigation Light Detection and Ranging (GEDI LiDAR), Sentinel-1, and Sentinel-2, with field measurement data to estimate above-ground biomass in the mangrove forest of Rawa Aopa Watumohai National Park (RAWNP), Indonesia. Data processing was performed using Google Earth Engine, model training was conducted in Google Colab, and spatial analysis was performed with QGIS. Mangrove cover was mapped using Normalized Difference Moisture Index (NDMI) and Modified Normalized Difference Water Index (MNDWI) to estimate mangrove area in RAWNP. Furthermore, machine learning models, including Random Forest (RF), Gradient Boosting, Extreme Gradient Boosting, and Support Vector Regression, were developed and validated based on 30 field plots and 10-fold cross-validation. A total of 2,176 GEDI footprint points were used as reference data for model training. The results showed that RF outperformed the other model, with R^2=0.46, Root Mean Square Error (RMSE)=72.52 during the evaluation stage and R^2=0.69, RMSE=29.47 during validation. Multitemporal analysis (2019-2023) showed peak above-ground biomass density in 2021 at 148.94 tons ha^{-1}, followed by a decline. This study presents an effective approach for estimating and mapping above-ground biomass in the mangrove forest of RAWNP, and the resulting biomass maps can be used to support mangrove conservation strategies, REDD+ verification, and coastal ecosystem management in tropical protected areas.

Keywords: Above-ground biomass, GEDI, machine learning, mangrove forest, Sentinel

INTRODUCTION

Mangrove forests play a vital role in climate change mitigation by storing carbon and stabilising coastal ecosystems (Hamuna et al. 2019; Simard et al. 2019), with biomass serving as a key indicator for assessing blue carbon services and informing carbon accounting for REDD+ and equitable policy design (Labriere et al. 2018; Mills-Novoa and Liverman 2019; Alongi 2020). Mangrove Above-Ground Biomass (AGB) is closely linked to biodiversity, as its structural complexity supports habitats for diverse fauna. Biomass changes affect shelter, breeding sites, and food availability, influencing species richness and ecosystem function (Maureaud et al. 2019; Bai et al. 2021; Arifanti et al. 2022). However, these ecosystems are increasingly threatened by natural and anthropogenic pressures, leading to functional and spatial decline, including in Rawa Aopa Watumohai Swamp National Park (RAWNP), Indonesia (Qiptiyah et al. 2013; Ridha et al. 2021).

Effective mangrove management requires biomass data that are accurate and timely (Indrayani et al. 2021), but while field inventories offer high accuracy (Sparks et al. 2024), they are costly and limited in coverage, especially in remote mangrove areas (Bruening et al. 2021; Goodbody et al. 2023). Integrating field data with satellite imagery offers a practical solution to overcome constraints such as data saturation, resolution limits, and atmospheric disturbances (Hernández-Stefanoni et al. 2020; Zhang et al. 2020; Hu et al. 2024; Shi et al. 2024).

One major advance in satellite-based forest monitoring is the Global Ecosystem Dynamics Investigation (GEDI) mission, which has provided AGB data globally since 2019 through spaceborne Light Detection and Ranging (LiDAR) (Dubayah et al. 2020). Sentinel-1 and Sentinel-2 are high-resolution, open-access Earth observation satellites (Nandy et al. 2021). Sentinel-1 uses C-band SAR radar that operates regardless of sunlight or weather, while Sentinel-2 captures multispectral data related to vegetation health and biomass (Askar et al. 2018; Zarco-Tejada et al. 2019). Combining structural data from Sentinel-1, spectral data from Sentinel-2, and GEDI as reference enables generation of spatially comprehensive biomass maps (Kacic et al. 2021; Xiao et al. 2022).

Although GEDI provides AGB reference data, Tamga et al. (2023) reported the limitations in various types of forest ecosystems with diverse densities. AGB estimation bias can also occur due to uneven footprint distribution and different data qualities at each GEDI trace point (Lang et al. 2022; Rishmawi et al. 2022; Bullock et al. 2023).

Therefore, AGB prediction model resulting from the integration of GEDI data and Sentinel imagery must be validated with field data to maintain accuracy (Zhou et al. 2025).

The integration of Machine Learning (ML) and the Google Earth Engine (GEE) platform has proven effective for biomass modeling and large-scale remote sensing data processing (Kumar and Mutanga 2018), including global applications using GEDI and Sentinel data (Gupta and Sharma 2022; Bullock et al. 2023; Lutz et al. 2024). However, applications in mangrove ecosystems remain limited, particularly due to the scarcity of locally specific AGB datasets. While deep learning is a powerful tool for biomass estimation (Oehmcke et al. 2022; Tian et al. 2024), it typically demands large training data, longer processing time, and complex interpretation. Hence, this study prioritizes conventional ML approaches, which are more efficient and interpretable for mangrove AGB modeling with limited data (London 2019; Wu et al. 2021).

Various approaches have been applied in mangrove AGB studies across Indonesia and Southeast Asia, including carbon stock recovery (Cameron et al. 2019), species-specific biomass contributions (Nur et al. 2022), and the use of Sentinel imagery combined with machine learning in areas such as Benoa and Komodo National Park (Rijal et al. 2023; Hidayah et al. 2024). However, most of these studies have not yet incorporated GEDI data. This integration is essential to improve mapping efficiency (Gouvêa et al. 2022; Winanti et al. 2023) and to support international reporting frameworks such as the United Nations Framework Convention on Climate Change (UNFCCC), Convention on Biological Diversity (CBD), and Sustainable Development Goals (SDGs) (Bunting et al. 2022).

This study focused on the mangrove forest in RAWNP, an important conservation area in the Wallacea Zone with high flora and fauna diversity (Ridha et al. 2021). The objective was to estimate and map mangrove AGB by integrating GEDI LiDAR, Sentinel data, and field measurement data using machine learning. The results are expected to provide accurate AGB information to support the development of more efficient estimation and mapping methods, particularly in the RAWNP area.

MATERIALS AND METHODS

Study area

This study was conducted in the Rawa Aopa Watumohai Swamp National Park (RAWNP) mangrove forest in Southeast Sulawesi Province, Indonesia, from January to June 2023. Mangrove in RAWNP stretches for ±24 km in the southern part of the area and covers an area of about 6,811 hectares. Geographically, the study area is located at 122.029°-122.168°E and 4.446°-4.604°S (Figure 1). This ecosystem is dominated by *Rhizophora mucronata*, *Avicennia alba*, *Bruguiera* spp., *Ceriops decandra*, *Lumnitzera* spp., *Sonneratia alba, Xylocarpus granatum, Acanthus ilicifolius, Acrostichum aureum,* and *Pandanus* sp.. The RAWNP is also home to a diverse range of wildlife, including estuarine crocodiles (*Crocodylus porosus*), anoa (*Bubalus depresicornis*), wild boar (*Sus scrofa*), mangrove crab (*Scylla serrata*), as well as waterfowl, namely snake pecking (*Anhinga melanogaster*), wilwo crane (*Mycteria cinerea*), and silver crane (*Egretta intermedia*).

Figure 1 presents the study area within the mangrove forest of RAWNP and the distribution of GEDI L4A footprint data. Figure 1.A shows the spatial boundary of the mangrove ecosystem in RAWNP, while Figure 1.B illustrates the distribution of GEDI footprint points used as reference AGB data. This visualization provides an overview of the spatial extent of the study area and the coverage of reference data used for biomass estimation. Clear presentation of the study area and GEDI distribution is essential to demonstrate the representativeness of the analysis and to establish the spatial basis for linking field-measured vegetation structure with remotely sensed data in the AGB modeling process.

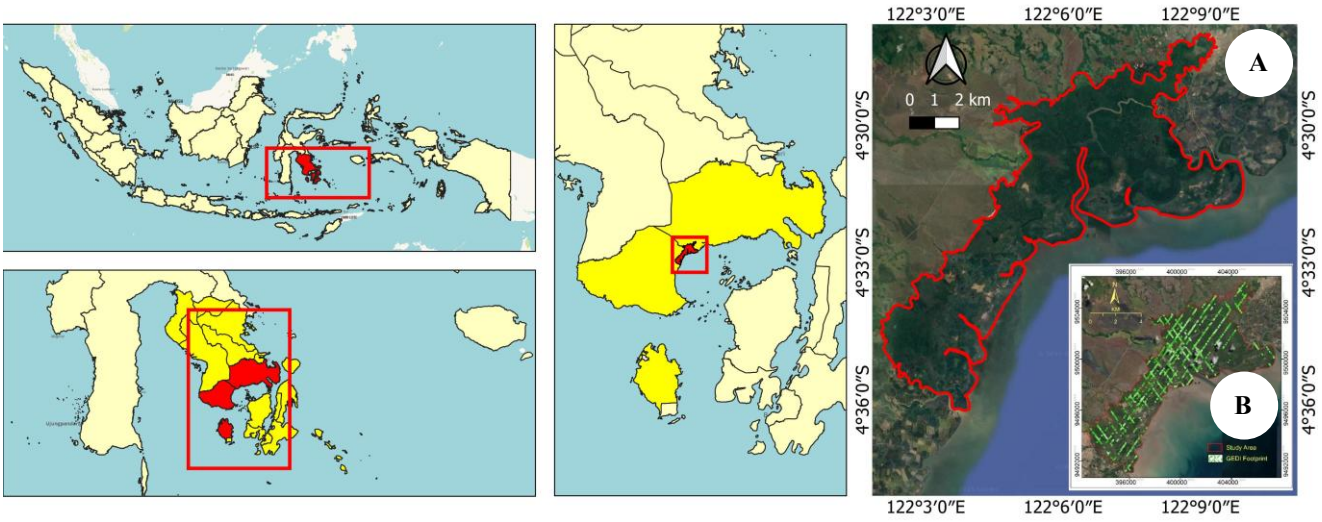

Figure 1. A. Study area, B. GEDI footprint in Rawa Aopa Watumohai Swamp National Park (RAWNP) mangrove ecosystem, Southeast Sulawesi Province, Indonesia

Data sources and analysis tools

The remote sensing data used consists of GEDI L4A (LiDAR-based AGB estimation, 25 m resolution), Sentinel-1 (SAR VV and VH for vegetation structures), Sentinel-2 (10-20 m multispectral imagery for reflectance and vegetation index analysis), and Copernicus GLO-30 DEM (30 m resolution for topographic information). Field AGB data were collected from 30 random plots (20×20 m), while mangrove ecosystem boundaries were obtained from the management authority of RAWNP (Table 1). GEE was used to collect, filter, mask, and compile annual median image composites. AGB modeling with ML was performed using Google Colab, while advanced spatial analysis was carried out using QGIS software. Figure 2 shows the study workflow, including the stages of multi-source data processing, development of machine learning models, and validation of prediction results using field data.

Figure 2 presents the complete workflow of this study, starting from data acquisition (Sentinel-1 and Sentinel-2 imagery, GEDI LiDAR data, and field plot measurements); then, moving through preprocessing and feature extraction, model training and validation using machine learning, and culminating in spatial mapping of AGB. The diagram is structured to illustrate the sequence of data integration and analytical processes applied throughout the study. Clarifying this workflow is essential for ensuring methodological transparency and enabling others to replicate the process in different mangrove forest areas using a similar method.

Remote sensing image acquisition and processing

This study integrated several remote sensing datasets. The following is an explanation of the acquisition and processing process.

Sentinel-1 image processing

Sentinel-1 data imported from GEE are Sentinel-1 Ground Range Detected (GRD), with Interferometric Wide (IW) acquisition mode, VV and VH polarization, and DESCENDING orbital path. After the data were filtered based on the period and study area, the backscatters were converted from a linear to a decibel (dB) scale to improve readability and compatibility in biomass analysis. Furthermore, texture analysis was performed using a Gray-Level Co-occurrence Matrix (GLCM) to extract additional features that can be used as predictors in AGB modeling. GLCM is a statistical method that measures texture by measuring the spatial relationship of pixel intensities, such as contrast, dissimilarity, Second Angular Moment, and Inverse Difference Moment (Chen et al. 2020). In radar-based biomass estimation, especially using Sentinel-1, texture metrics from GLCM can improve model performance by revealing patterns that are not captured by backscatter intensity alone (Munthe and Sulistiyono 2023). Before being exported to GEE assets, Sentinel-1 data were combined using an annual median value to obtain a representative value.

Sentinel-2 image processing

Sentinel-2 Surface Reflectance (COPERNICUS/S2_SR_HARMONIZED) data were imported from GEE and filtered by period and study area. Reflectance correction was performed by converting the Digital Number (DN) value to a reflectance value on a scale of 0-1. Cloud masking was implemented using the Cloud Score Plus (CS+) algorithm to ensure that only cloud-free pixels were used. The CS+ algorithm is a cloud detection method in Google Earth Engine that refines the original cloud score algorithm by improving discrimination between clouds and bright surfaces (Kumar and Mutanga 2018). It uses a composite of spectral thresholds and was developed for more accurate preprocessing of Sentinel-2 data (Bezerra et al. 2023).

In addition to the single reflectance band values of Sentinel 2, Vegetation indices are also extracted from the main bands using the equations as shown in Table 2. The values of these indices also serve as predictor features of the AGB model, which include Normalized Difference Vegetation Index (NDVI), Enhanced Vegetation Index (EVI), Soil Adjusted Vegetation Index (SAVI), Modified Normalized Difference Water Index (MNDWI), Moisture Stress Index (MSI), Normalized Difference Moisture Index (NDMI), Ratio Vegetation Index (RVI), and Red Edge NDVI, which were calculated from the main band. Subsequently, the data were composited using an annual median to reduce the influence of noise and temporal variability before being exported to GEE Assets.

DEM-based slope extraction

Slope data were extracted from the Digital Elevation Model (DEM) Copernicus GLO-30 DEM (COPERNICUS/DEM/GLO30). Before slope data were extracted, DEM data were filtered by study area and then cut according to the study area limits. The resulting slope map was used as a filtering criterion to exclude GEDI footprints located in steep terrain (>30°), which are known to reduce LiDAR accuracy in biomass estimation (Wang et al. 2023). This topographic constraint was also used to ensure consistency with previous studies and enhance model reliability (Ni et al. 2021).

Table 1. Summary of the data used in this study

Data types	Source	Spatial resolution	Period
GEDI L4A	NASA GEDI	25 m	2019-2023
Sentinel-1 SAR	ESA Copernicus	10 m	2019-2023
Sentinel-2 Multispektral	ESA Copernicus	10-20 m	2019-2023
Digital Elevation Model (DEM)	ESA Copernicus GLO-30	30 m	-
Field-measured AGB	Field measurement	Plot 20 m × 20 m	2023
Mangrove Ecosystem Boundary Shapefile	Management Authority of RAWNP		2023

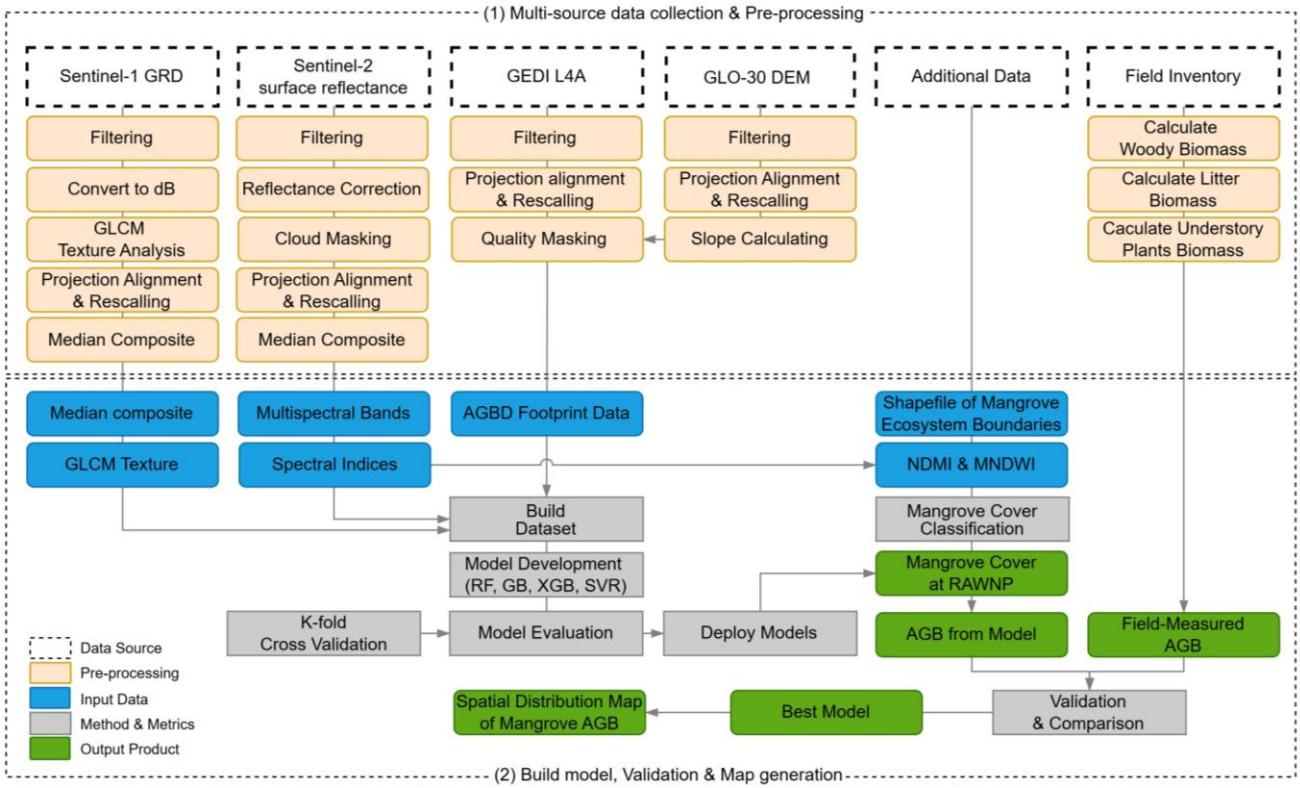

Figure 2. Study workflow

GEDI data filtering and preprocessing

GEDI L4A data were obtained from the GEE database of the LARSE/GEDI/GEDI04_A_002_MONTHLY collection. The data were screened by the period and area of the study, with the selection of quality flag data = 1 and degrade_flag = 0 to ensure that only high-quality AGB estimation data were used. Additional selection was applied by filtering the data with an estimated error rate (AGB_se/AGB≤0.20) and considering a land slope <30° to improve the accuracy of the model. These three parameters are the standard for filtering GEDI data in many studies that are commonly used to ensure that only high-quality GEDI data is used in the analysis. This is also related to consistency between studies. As for filtering based on other attributes, such as sun elevation, we did not use it, because GEDI uses active LiDAR (not passive sensors such as optics), so it does not depend on sunlight. Where observations were made both day and night, there was no significant difference in waveform quality (Liu et al. 2021; Moudrý et al. 2024). The selected data were then composited using the mosaic method before being exported to GEE Assets. From this process, 2176 footprint points containing AGB data from GEDI-L4A were collected. These points were spread across the research locations and will be used as target data to build an AGB estimation model in mangrove forests with predictor features derived from Sentinel imagery.

The entire dataset (Sentinel-2, Sentinel-1, GEDI, and DEM) was aligned in UTM coordinate system Zone 51S (EPSG:32751) and adjusted to a spatial resolution of 20 m using the reprojection method to be compatible with AGB modeling. Sentinel-2 was used as a pixel grid reference, while Sentinel-1, DEM, and GEDI were projected to align using Sentinel-2 was used as a pixel grid reference, while Sentinel-1, DEM, and GEDI were projected to align using the same reference system. Export parameters to the same reference system. Export parameters (crs: EPSG:32751, scale: 20) were applied to maintain the suitability of the resolution and projection system for the entire dataset.

Field AGB measurement

Field AGB data were used to validate the model AGB data built from GEDI L4A and Sentinel data. The measurement data were collected from 30 random sample plots at the study site. In general, field AGB is the accumulation of tree biomass (AGB), litter biomass, and undergrowth biomass (BKT), expressed in tons ha^{-1}. Tree biomass was calculated using a global allometric model developed by Chave et al. (2005) to estimate AGB in mangrove forests:

$$AGB = 0.0673 (\rho D2H)^{0.976} \quad [1]$$

Where:

AGB: Biomass of fluff (kg)

D : Diameter (cm)

H : Height (m)

ρ : Specific gravity (grams/cm^3) obtained from (Zanne et al. 2009)

The calculation of litter and undergrowth biomass (BKT) used the general formula:

$$BKT = \frac{BKC}{BBC} \times BBT \quad [2]$$

Where:
BKT : Oven dry weight (kg)
BKC : Dry weight of sample (kg)
BBC : Wet weight of sample (kg)
BBT : Total wet weight (kg)
Therefore, AGB was calculated using the equation:

$$AGB = \frac{AGB + BKT}{Lp} \quad [3]$$

Where:
BIO : Total biomass (kg ha^{-1}), kg divided by 1000 (converted to tons ha^{-1})
AGB: Above-ground biomass (kg)
BKT : Biomass of litter and plants (kg)
Lp : Plot area (ha)

Limited accessibility at the study site posed a particular challenge for field data collection. Although the number of field plots was relatively small (30 plots), they were randomly placed to ensure that the samples could optimally capture the variability of ecosystem conditions. This field plot is used exclusively to validate independently predicted AGB values. The AGB modeling was developed using GEDI L4A trace data (n = 2,176), which were associated with predictor features derived from Sentinel-1 and Sentinel-2 imagery.

Figure 3 illustrates the spatial distribution and plot design used for above-ground biomass measurement in the field. Figure 3.A shows the location of 30 sampling plots distributed across the mangrove ecosystem in RAWNP, representing spatial variability in stand structure. Figure 3.B presents the standard 20×20 m plot layout, which is subdivided into nested subplots for measuring vegetation at different growth stages. The 20×20 m area is used to measure trees with a diameter of ≥20 cm (tree phase), while 10×10 m subplots are used for poles with diameters between 10 cm and <20 cm (pole phase). The 5×5 m subplots are designated for saplings with diameters <10 cm and height ≥1.5 m (sapling or "pancang" phase), and 1×1 m subplots are used to assess seedlings with height ≤1.5 m (seedling or "*semai*" phase) as well as litter and understory vegetation. This stratified design ensures that AGB estimates capture all vegetation strata accurately and representatively.

Mangrove mapping and classification

Mangrove cover mapping was carried out using two spectral index from Sentinel-2, namely Normalized Difference Moisture Index (NDMI) and Modified Normalized Difference Water Index (MNDWI) (Hickey and Radford 2022; Suyarso and Avianto 2022). This was achieved by applying NDMI thresholds of > 0.3 and MNDWI ≤ 0, which represent vegetation with high levels of humidity without the presence of a dominant water body (Otero et al. 2020; Pena-Regueiro et al. 2020; Sudirman et al. 2023). NDMI is highly sensitive to vegetation moisture and effectively detects mangrove ecosystems with high moisture content (Suyarso and Avianto 2022). MNDWI separates aquatic objects from vegetation and terrestrial land (Pena-Regueiro et al. 2020). The results of this classification were then overlaid with RAWNP mangrove ecosystem boundaries (shapefile), and mangrove cover area was calculated by converting the number of pixels classified as mangrove to hectares.

AGB modeling with machine learning

AGB modeling was performed using machine learning, in which AGB GEDI was used as a target variable (dependent variable), with Sentinel-1 and Sentinel-2 being independent variables. In this study, feature selection was carried out using RandomForestRegressor, and a threshold value of ≥0.01 was applied to avoid potential overfitting and maintain features contributing to AGB estimation. A summary of the features used in this study is provided in Table 2.

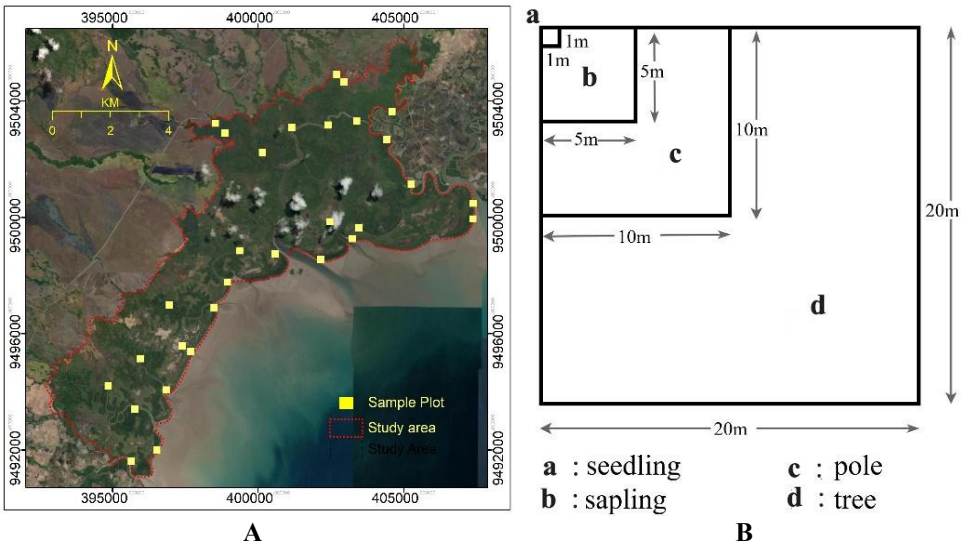

Figure 3. A. Sampling plot distribution in the study area, B. Nested plot design: a. (1×1 m, seedlings), b. (5×5 m, saplings), c. (10×10 m, poles), d. (20×20 m, trees)

Table 2. Predictor features used in this study

Source image	Variable	Description/Equation
Sentinel-1 polarization	VV	Vertical transmit-vertical channel
	VH	Vertical transmit-Horizontal channel
Sentinel-1 texture	VV_con, VH_con	GLCM Contrast
	VV_diss, VH_diss	GLCM Dissimilarity
	VV _asm, VH _asm	GLCM Angular Second Moment
	VV_idm, VH _idm	GLCM Inverse Difference Moment
	VV_var, VH _var	GLCM Variance
Sentinel-2	B2	Blue, 490 nm (B)
Multispectral bands	B3	Green, 560 nm (G)
	B4	Red, 665 nm (R)
	B5	Red edge, 705 nm (RE5)
	B6	Red edge, 749 nm (RE6)
	B7	Red edge, 783 nm (RE7)
	B8	Near Infrared, 842 nm (NIR)
	B8a	Near Infrared, 865 nm (NNIR)
	B11	Short Wave IR, 1610 nm (SWIR1)
	B12	Short Wave IR, 2190 nm (SWIR2)
Sentinel-2 vegetation indices	EVI	$2.5 \text{ x } \frac{(\text{NIR} - \text{R})}{(\text{NIR} + (6\text{xR})) - ((7.5\text{xB}) + 1)}$
	MNDWI	$\frac{(\text{G} - \text{SWIR1})}{(\text{G} + \text{SWIR1})}$
	MSI	$\frac{\text{SWIR1}}{\text{NIR}}$
	NDBI	$\frac{(\text{SWIR1} - \text{NIR})}{(\text{SWIR1} + \text{NIR})}$
	NDMI	$\frac{(\text{SWIR1} - \text{NIR})}{(\text{SWIR1} + \text{NIR})}$
	NDVI	$\frac{(\text{NIR} - \text{R})}{(\text{NIR} + \text{R})}$
	NDVI5	$\frac{(\text{NIR} - \text{RE5})}{(\text{NIR} + \text{RE5})}$
	NDVI6	$\frac{(\text{NIR} - \text{RE6})}{(\text{NIR} + \text{RE6})}$
	NDVI7	$\frac{(\text{NIR} - \text{RE7})}{(\text{NIR} + \text{RE7})}$
	RVI	$\frac{\text{NIR}}{\text{R}}$
	SAVI	$1.5 \text{ x } \frac{(\text{NIR} - \text{R})}{(\text{NIR} + \text{R} + 0.5)}$

Note: MSI: Moisture Stress Index, NDBI: Normalized Difference Built-up Index, NDMI: Normalized Difference Moisture Index, NDVI: Normalized Difference Vegetation Index, NDVI5: Normalized Difference Vegetation Index (Band 5 and 4), NDVI6: Normalized Difference Vegetation Index (Band 6 and 4), NDVI7: Normalized Difference Vegetation Index (Band 7 and 4), RVI: Ratio Vegetation Index, SAVI: Soil Adjusted Vegetation Index

After the predictor feature was selected, each machine learning model was trained and evaluated using a 10-fold cross-validation scheme applied to the entire dataset. In this approach, the model is iteratively trained on 90% of the data and tested on the remaining 10% in each fold, ensuring that all data points are used for both training and testing. Four machine learning algorithms were used in the model training process, namely Random Forest (RF), Gradient Boosting (GB), Extreme Gradient Boosting (XGB), and Support Vector Regression (SVR). These four algorithms have the advantage of identifying complex data patterns and handling nonlinear relationships (Moradi et al. 2023; Rocha et al. 2023). A 10-fold cross-validation method was applied during the evaluation stage to avoid overfitting and improve model generalization. The performance of the model is the average performance from all iterations. Several evaluation metrics are used to measure model performance, such as the determination coefficient (R-squared/R^2), Root Mean Square Error (RMSE), Mean Absolute Error (MAE), and bias (Luo et al. 2024).

Model validation

Model validation was performed by comparing the value of AGB from the model prediction with field measurements to assess the accuracy (Yu et al. 2021). The validation data used are AGB values from 30 plots resulting from field measurements, which are used specifically for independent validation and are not involved in the model training process. The validation results'

accuracy was measured using R^2, RMSE, and residual analysis results. In AGB modeling, R^2 value indicates the extent to which the model can explain the target data (AGB) (Stoffel et al. 2021). Meanwhile, RMSE shows the average value of the deviations from the prediction results, which deviates from the reference data. AGB results were obtained from field measurements (Saldaña-Villota and Cotes-Torres 2021). The residual is the difference between the reference and model-predicted AGB, which indicates the magnitude and direction of the bias, whether underestimated or overestimated (Picard et al. 2025).

AGB mapping and multi-temporal analysis

AGB mapping and multi-temporal analysis were carried out by applying the best AGB model to Sentinel imagery from 2019 to 2023. This comprehensive analysis included AGB estimation at the pixel level, making it possible to perform multi-temporal analysis with high resolution. The mapping results provide detailed information on the spatial distribution of AGB each year and the changing trends. The calculation for each year was carried out using zonal statistics, which included estimates of minimum, maximum, average, and standard deviation of AGB to assess biomass variation between years. The prediction results were visualized in the form of an annual thematic map, using a gradation color scale to illustrate changes in mangrove biomass density. Temporal trend analysis identified patterns of change in biomass annually, both influenced by natural factors, such as vegetation growth and ecosystem succession, along with anthropogenic factors, namely deforestation and land conversion.

RESULTS AND DISCUSSION

Spatial distribution of mangrove cover

Spatial distribution of mangrove cover in RAWNP was analyzed using NDMI and MNDWI spectral indices from Sentinel-2 images. Mangrove cover area fluctuated during 2019–2023, based on the classification results (Figure 4). In 2019, the area of mangrove was recorded at 5,842.94 Ha, increasing to 6,050.94 Ha in 2020 and reaching the peak in 2021 (6,161.75 Ha) and 2022 (6,183.94 Ha). However, in 2023, the area decreased to 5,942.31 Ha, a reduction of 241.63 Ha compared to the previous year.

Spatially, the mangrove cover map (Figure 4) shows that areas with increasing and decreasing mangrove cover were uneven across RAWNP area. Some areas are experiencing mangrove expansion, while others are witnessing degradation that could be caused by anthropogenic activity, changes in coastal hydrodynamics, or ecological disturbances, such as abrasion and sedimentation. These fluctuations in mangrove cover can be attributed to environmental factors and ecosystem management (Arifanti et al. 2022). An upward trend through 2022 may indicate the effectiveness of natural conservation and regeneration of mangrove ecosystems, while a widespread decline in 2023 could be due to a combination of factors such as climate change (e.g., rising temperatures and extreme rainfall), land-use changes, and pressures from economic activities around RAWNP area (Utami et al. 2024b). Further study is required to evaluate the impact of these factors on the long-term survival of mangrove ecosystems.

Fluctuations in mangrove cover area in RAWNP that occurred during the 2019-2023 period are in line with a study by Arifanti et al. (2022), which stated that mangrove cover generally increases through rehabilitation activities. However, it is also highly susceptible to decline due to land conversion and hydrological changes. Utami et al. (2024b) also emphasize that coastal community activities and local climate change essentially trigger the degradation of national mangroves. Patterns of degradation that are generally found in mangrove edge areas and stability in the central region of mangrove areas were also reported by Rudianto et al. (2020) in mangrove forests on the coast of East Java.

Predictor feature selection

The results showed that 29 features were selected as predictors in building the AGB estimation model. Features B12, VV, and B5 generally had the highest essential feature values (Figure 5). The B12 (28.21) can capture moisture variations in leaves and soil, which is significantly related to biomass. (Masiello et al. 2022). VV polarisation, with the ability to capture information on the vertical structure of the forest (Narvaes et al. 2023), had a considerable significance value of 10.83. Moreover, B5 has sensitive characteristics of chlorophyll content and plant health (Coetzee 2022) had a significant value of 4.97 compared to other features.

Some features, such as NDVI_5, MNDWI, and Sentinel-1 texture features, also contribute significantly to the model. The feature NDVI_5 is that the red edge band has a high sensitivity to chlorophyll, making it superior in detecting biomass of dense vegetation such as mangroves (Bezerra et al. 2023). MNDWI has proven to be very efficient in extracting the main features of water-covered areas compared to other indices (İspir 2025). Meanwhile, the textural features of Sentinel-1, such as contrast and entropy, correlate with biomass through their ability to depict spatial variation and complexity of vegetation structure (Argamosa et al. 2018). Other features have low essential values but are retained because they are relevant to improving the accuracy of AGB estimation.

AGB model development

AGB model development uses selected features, resulting in varied performances. Figure 6 shows the performance of each model during the iteration process using the 10-fold cross-validation method. For R^2 metric (Figure 6.A), RF model consistently showed the highest value at 9-fold, followed by GB and XB, with R^2 slightly below RF, while SVR had the lowest value for all folds. Similarly, for RMSE metric (Figures 6.B and 6.C), RF, GB, and XB showed relatively low and stable errors in almost all folds, except for fluctuations in fold four and drastic decreases in fold ten. SVR showed a significantly higher RMSE, reaching >100 tons/ha in the 4th fold. The same pattern was shown in MAE metrics, where RF, GB,

and XB had minor and consistent mean absolute errors compared to SVR. On the bias metric (Figure 6.D), all models showed a negative bias or tendency to underestimate AGB. SVR demonstrated the most considerable bias, while RF, GB, and XGB had a relatively small bias close to 0 on the 9th and 10th folds.

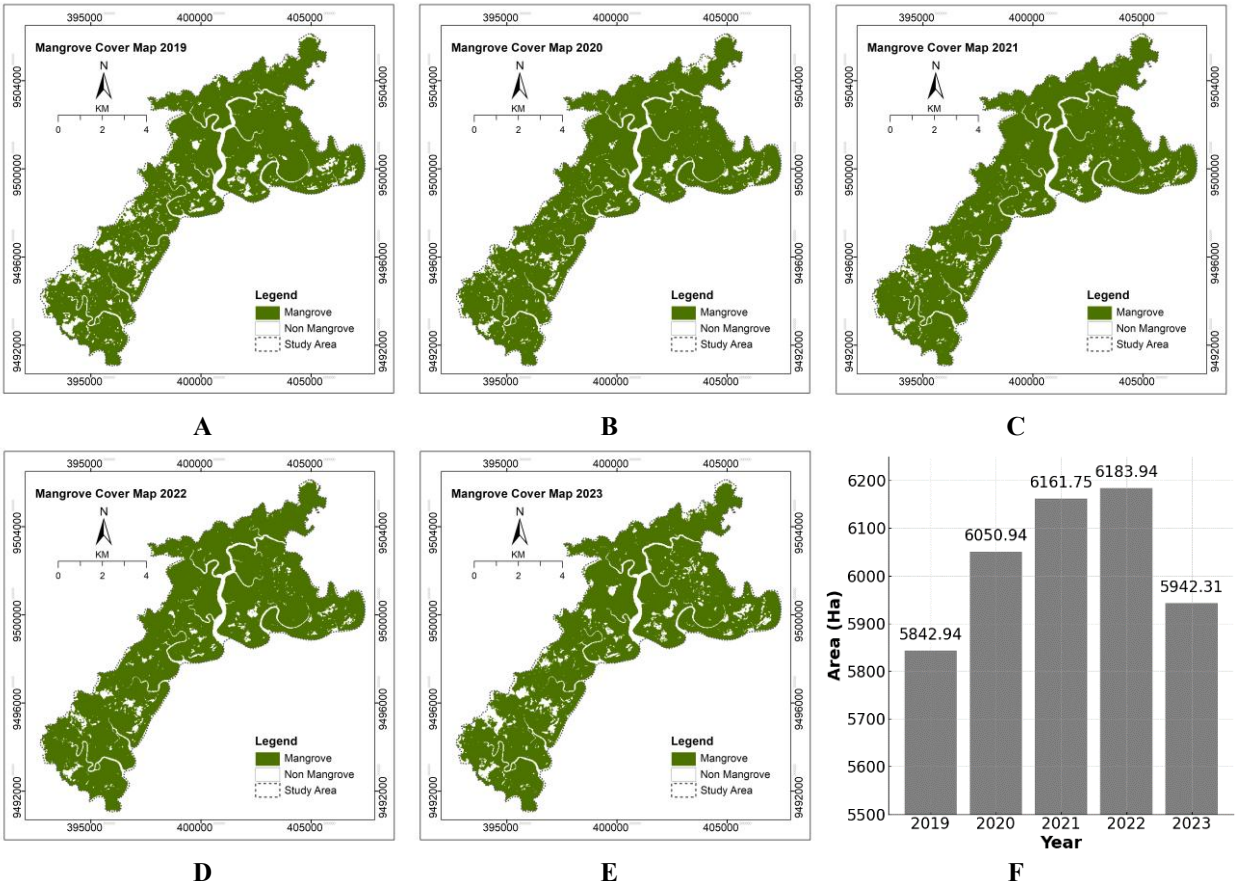

Figure 4. Mangrove cover in Rawa Aopa Watumohai Swamp National Park (RAWNP), Indonesia. A. 2019, B. 2020, C. 2021, D. 2022, E. 2023, F. Dynamics of mangrove forest area

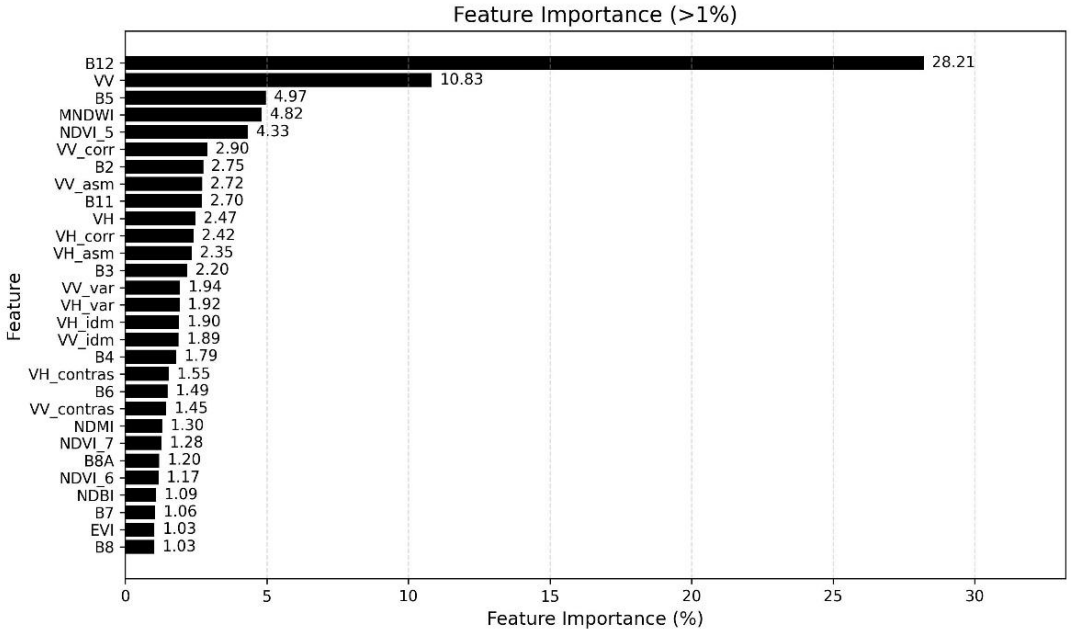

Figure 5. Essential features for above-ground biomass prediction models

The 10-fold cross-validation method is applied in this study not only to assess model performance but also to reduce the risk of overfitting (Yates et al. 2023). This is because this method provides certainty for each data point to be used, both as training data and test data, in different iterations. The evaluation results, which are the average of the evaluation values at each iteration, also provide more reliable stability than the single data division method (Budiman 2019). This approach is very useful when working with heterogeneous ecological data, such as in multi-sensor image-based AGB modeling (Ploton et al. 2020). In addition to cross-validation, bias analysis is also applied as an important diagnostic metric to detect model imbalance, especially when working with heterogeneous and nonlinear datasets. In ensemble models such as RF, GB, and XGB, the use of bias analysis complements error metrics (e.g., RMSE, MAE) by revealing directional tendencies in the prediction results (Luo et al. 2024). This step is essential to ensure model robustness and to avoid misleading conclusions.

Table 3 shows a summary of the performance of each model for all evaluation metrics. RF model had the best results in the three evaluation metrics, with the highest R^2 value of 0.457, indicating the ability to explain approximately 46% of the variation in AGB data. RF also had the lowest RMSE and MAE values, which indicated better accuracy than the other models. RF bias value at-13.4 tons/ha was slightly higher than GB and XGB, suggesting a tendency to underestimate AGB. Both GB and XGB generally have a competitive performance, with evaluation metric values that are close to RF. Meanwhile, SVR showed the lowest value of all evaluation metrics, indicating a low ability to explain the variation of AGB data and a large error rate in prediction.

The low performance of the SVR in this study may be due to its limited flexibility in handling high-dimensional nonlinear datasets such as those derived from satellite imagery. SVRs are usually determined by a small set of hyperparameters and fail to capture complex ecological relationships from remote sensing data (López-Serrano et al. 2020). Additionally, SVRs are more sensitive to feature scaling and kernel selection, and may not be well generalized without extensive tuning (Qian et al. 2023). This is inversely proportional to ensemble models such as RF, GB, and XGB, which tend to be more resilient when dealing with multi-source predictive data that has a lot of distortion and uncertainty (Moradi et al. 2023; Rocha et al. 2023).

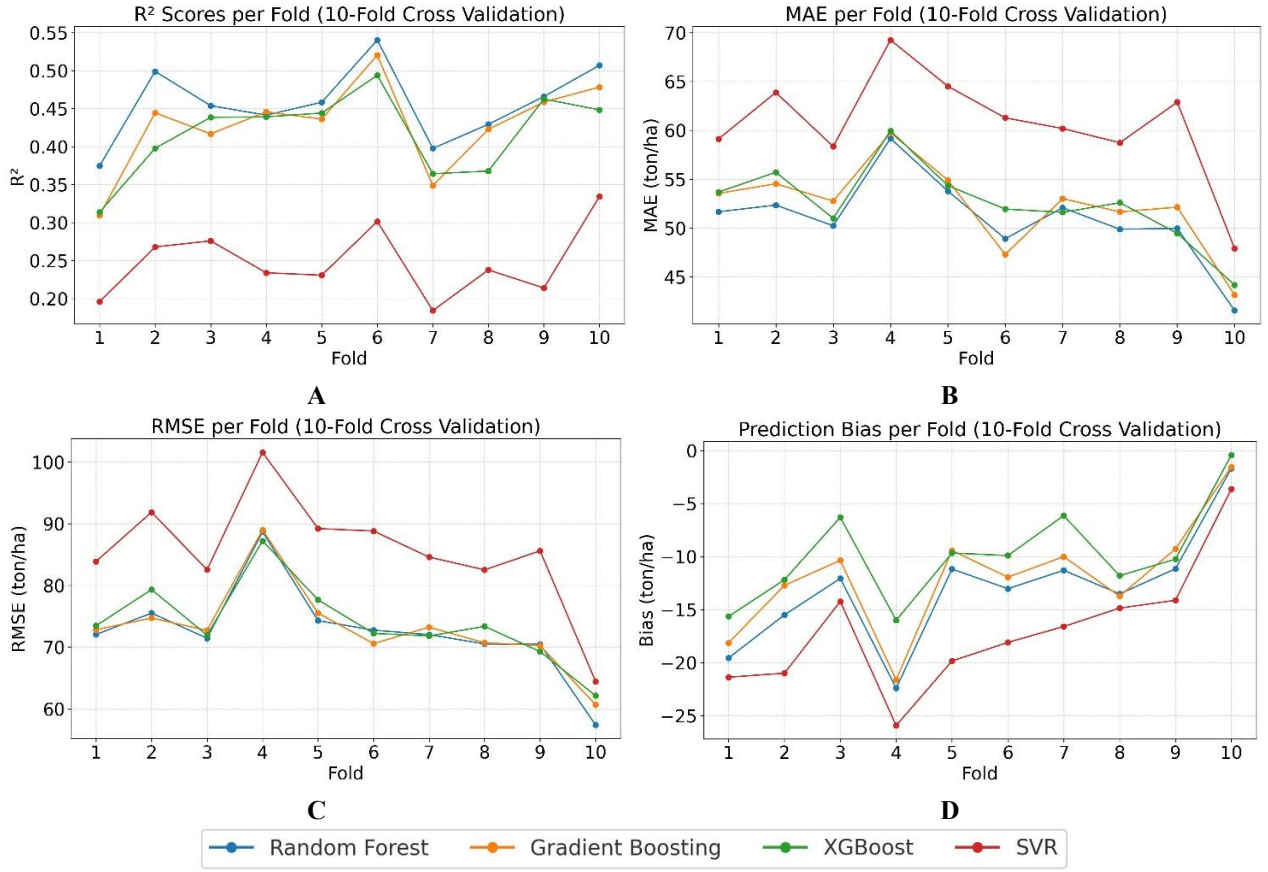

Figure 6. 10-fold cross-validation on various evaluation metrics. A. R^2, B. RMSE, C. MAE, D. Bias

Visually, the advantage of RF model at the evaluation stage is shown in Figure 7, illustrating the distribution of prediction results closest to the ideal line. GB and XGB showed a similar pattern to RF, while SVR had more significant deviations from the perfect line, indicating a higher rate of prediction error in AGB estimate. Overall, the evaluation results show that the RF-based model shows the most stable and accurate performance. This is in line with the research of Hu et al. (2020), which shows the effectiveness of RF in mapping global mangrove AGB. This is also supported by Pham et al. (2019), who advocate using RF because it is more adaptive in absorbing nonlinear and multicollinear variables, which are commonly found in biomass prediction based on satellite imagery.

Although this study shows an effective approach in estimating mangrove biomass, several things need to be examined more deeply as material for the development of watertight research. The sensitivity of the NDMI and MNDWI indices to fluctuations in humidity and tides can affect the results of mangrove classification in the tidal zone (Habibullah et al. 2023; Rondon et al. 2023). In addition, the uneven distribution of GEDI's footprint and the limited number of field plots also have the potential to cause spatial bias, especially in locations with extreme mangrove density (Marselis et al. 2020). Further studies are therefore recommended to integrate additional data such as UAV-LiDAR and tidal data. The increase in the number of field plots and the application of more complex models, such as deep learning, that can capture the details of data complexity, needs to be balanced to improve the accuracy of modeling results (Budiman et al. 2021). Future studies are recommended to increase the number and spatial distribution of field plots to enhance data representativeness and improve model accuracy.

Table 3. Model performance based on evaluation metrics at the evaluation stage

Model	R^2	RMSE (ton/ha)	MAE (ton/ha)	Bias (ton/ha)
RF	0.457	72.52	50.96	-13.14
GB	0.428	73.02	52.27	-11.88
XGB	0.417	73.85	52.44	-9.83
SVR	0.248	85.51	60.61	-16.97

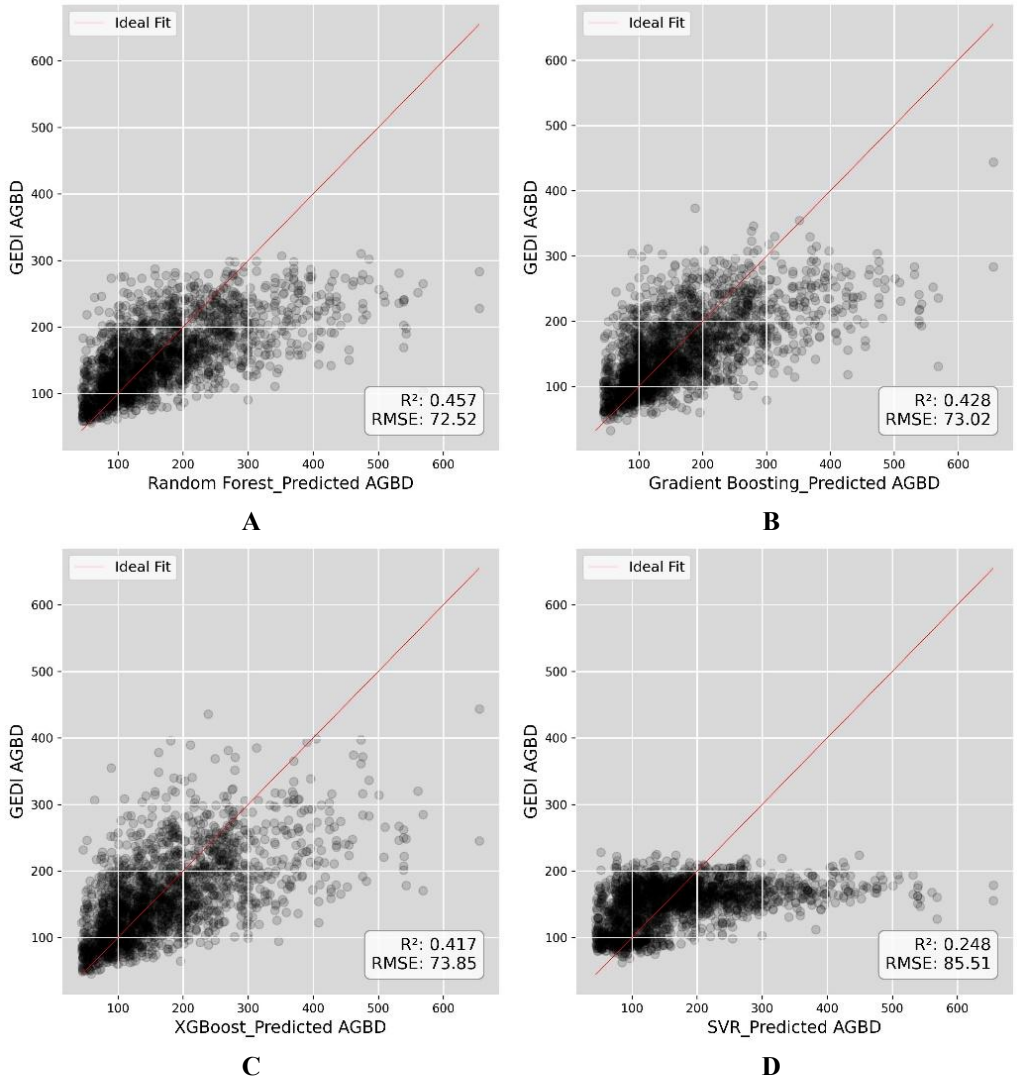

Figure 7. Scatterplot GEDI AGB vs Predicted AGB with A. RF, B. GB, C. XGB, D. SVR

Model validation

Differences in resolution and atmospheric influence on multispectral data can affect the estimated AGB. Therefore, model validation is an important stage to ensure accuracy (Rengarajan and Schott 2018; Bullock et al. 2023). Table 4 shows a summary of the model performance during the validation stage. RF model had the best performance, with a value of R^2 0.691 and RMSE of 29,474 tons/ha. XGB and GB models also performed well in the validation stage, with R^2 values of 0.589 and 0.563, respectively, as well as RMSEs of 33.32 tons/ha and 35.5 tons/ha. Meanwhile, SVR showed the lowest performance, with R^2 0.453 and RMSE of 39.22 tons/ha, indicating that this model is less effective in predicting AGB.

Figures 8.A-D shows the performance of each model at the data validation stage, which includes scatter plots, residual graphs, residual distributions, and line plots of prediction vs AGB validation. RF model visualizes the best accuracy with a data distribution close to the ideal line. The residual distribution is relatively symmetrical and close to normal, and tends to be concentrated around zero. The prediction plot line vs AGB validation is the most aligned with the data trends, which indicates the consistency of RF in capturing the actual tides of AGB, although there is a slight deviation in the peak value. The GB model tends to be unresponsive to extreme values, and XGB is more adaptive to variations in actual AGB data, but it produces fluctuations that are often too sharp in some data, leading to overfitting. SVR showed the lowest performance in all visualizations. Based on the results, RF is the most reliable model for AGB estimation, while SVR cannot represent the data structure complexity.

RF, GB, and XGB are ensemble models that can handle nonlinear, multicollinearity relationships between features at large data scales, such as AGB datasets (Gu et al. 2022; Manley et al. 2023; Wang 2024). RF algorithms are more stable options without complicated parameter tuning, while GB and XGB require more specific parameter tuning to achieve optimal results (Othman et al. 2023; Mosfeldt et al. 2024). SVR often encounters obstacles when dealing with high-dimensional datasets, making it less efficient (Xu et al. 2022; Roozbeh et al. 2023). Previous studies have also shown the effectiveness of RF models in estimating AGB. Liu et al. (2022) found that RF model provided the best biomass estimation results when analyzing several different tree types compared to backpropagation neural networks. A study conducted by Alvarez et al. (2012) reported that RF could bridge the gap between field measurements and remote sensing data, significantly improving the overall biomass estimation. Furthermore, Tavasoli and Arefi (2021) compared the capabilities of Synthetic Aperture Radar (SAR) and optical data in biomass mapping. The results showed that RF model led to a substantial reduction in RMSE compared to standard regression models. Bao and Huong (2025) also showed the superiority of RF for AGB estimation in Vietnam's Central Highlands using Landsat 8 satellite imagery.

Spatial distribution and temporal trends of AGB

The analysis results for the 2019-2023 period show fluctuations in the value of AGB with a dynamic pattern. Table 5 shows the results of the annual AGB prediction using an RF model.

The prediction results show that the highest average AGB occurred in 2021 at 148.94 tons ha^{-1}, while the lowest value was recorded in 2022 at 145.07 tons ha^{-1}, with a range between 51-443 tons ha^{-1}. An upward trend was recorded in the 2019-2021 period, indicating an improvement in ecosystem conditions and the possibility of natural recovery or regeneration. However, a gradual decline in 2022 and 2023 may suggest ecological and anthropogenic pressures on RAWNP mangrove ecosystems (Utami et al. 2024a).

Fluctuations in AGB values are observed in standard deviations, with the highest values in 2019 (58.17) and the lowest in 2022 (48.75), reflecting the dynamics of the spatial heterogeneity of mangrove ecosystems. A high standard deviation value indicates the presence of areas with high biomass adjacent to low-biomass zones, reflecting high variation in vegetation structure (Jantol et al. 2023). The decrease in standard deviation values in 2022 is likely due to the homogenization of stand structures, including the loss of large trees, which significantly reduces the variability of AGB between areas (Bai et al. 2021).

Figure 9 shows that areas with high AGB are less likely to experience changes or have consistent patterns. Spatial fluctuations in annual AGB generally occur in peripheral areas, specifically those with low biomass density. These results are consistent with those of Rudianto et al. (2020), who stated that coastal areas are vulnerable to anthropogenic disturbances, such as the expansion of ponds, settlements, and aquaculture activities, capable of decreasing mangrove biomass productivity.

Table 4. Model performance based on evaluation metrics at the evaluation stage

Model	R^2	RMSE (ton/ha)	MAE (ton/ha)	Bias (ton/ha)
RF	0.691	29,474	22,903	-4,552
GB	0.589	35,053	27,524	-11,656
XGB	0.563	33,979	26,029	-6,234
SVR	0.453	39,216	28,263	-6,747

Table 5. Prediction of AGB in Rawa Aopa Watumohai Swamp National Park (RAWNP) mangrove forest, Indonesia in 2019-2023

Year	Average AGB (ton ha^{-1})	Total AGB (ton)	AGB min (ton ha^{-1})	AGB max (ton ha^{-1})	Standard deviation
2019	148.71	796,865.29	51.33	443.89	58.17
2020	148.16	830,172.94	52.07	399.38	53.10
2021	148.94	863,057.51	52.61	354.92	53.61
2022	145.07	855,574.00	53.41	422.31	48.75
2023	145.69	794,402.20	51.66	348.77	56.44

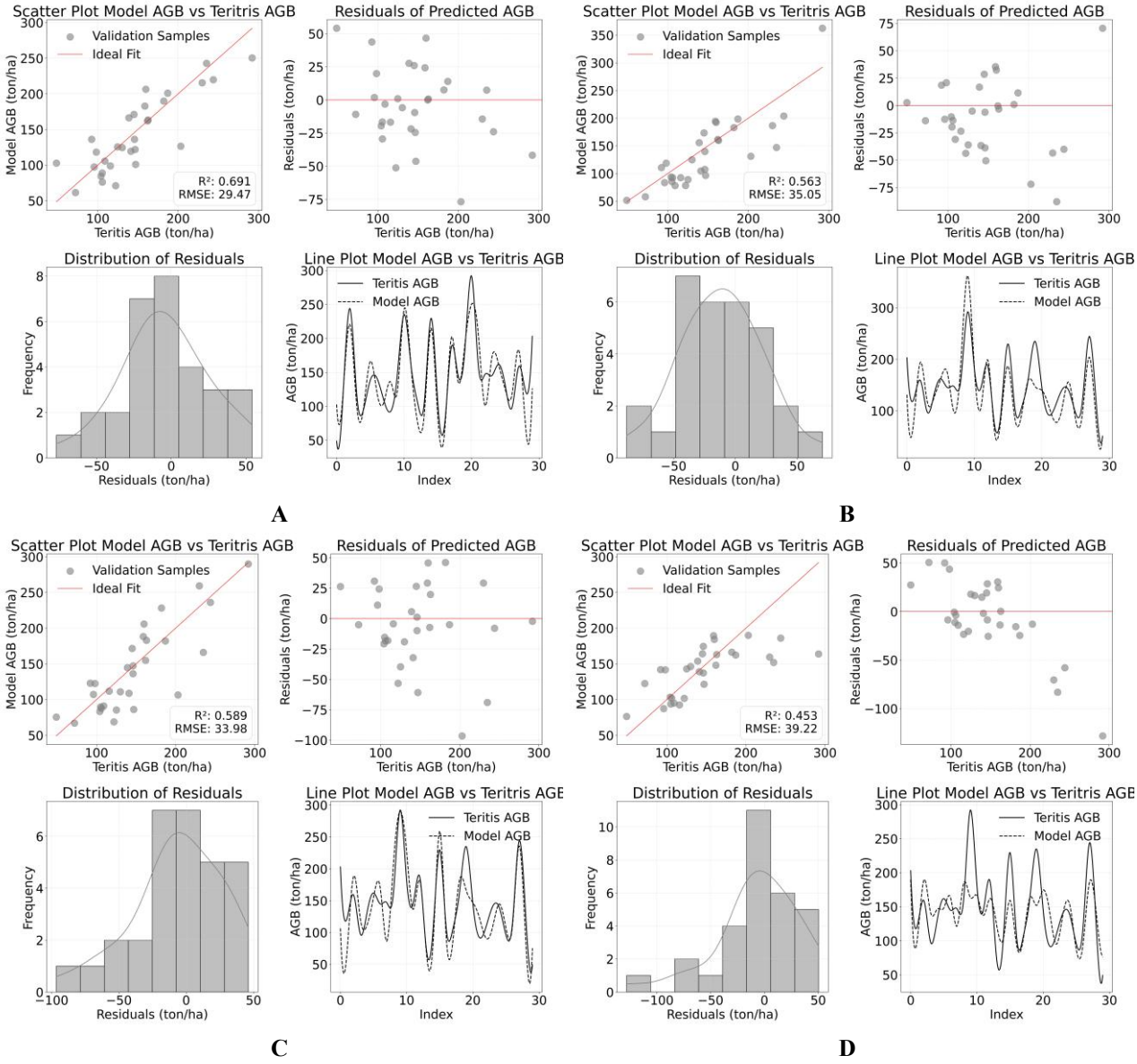

Figure 8. Visualization of model validation results. A. RF, B. GB, C. XGB, D. SVR

In addition to anthropogenic factors, AGB fluctuations, especially in the 2022-2023 period, are also likely to be caused by climate anomalies. Extreme La Niña conditions that last until the end of 2022 and early 2023 are likely to cause increased rainfall and flood intensity, which can have a negative impact on mangrove biomass by changing salinity gradients and increasing physical disturbances in coastal areas (Huang et al. 2024).

The decline in mangrove forest biomass is a complex problem generally caused by a combination of anthropogenic factors. The most significant cause is converting mangrove land into agricultural land, settlements, or pond cultivation (Sasmito et al. 2019). One of the derivative impacts is the decline in biodiversity, which indirectly affects biomass due to the disruption of the biogeochemical cycle in the mangrove forest (Carugati et al. 2018). Habitat fragmentation also causes a decrease in connectivity between parts of the mangrove forest, thereby hindering the ability to maintain biomass production and biodiversity (Bryan-Brown et al. 2020). Pollution from the use of chemicals for shrimp farming, agriculture, and industrial waste disposal, as stressed by Suwanto et al. (2021), has a severe negative impact on the health of mangrove and the accumulation of biomass. Fluctuations in soil salinity due to mangrove conversion significantly cause osmotic stress that affects water absorption ability, potentially reducing biomass growth and productivity (Devaney et al. 2021; Matto et al. 2023).

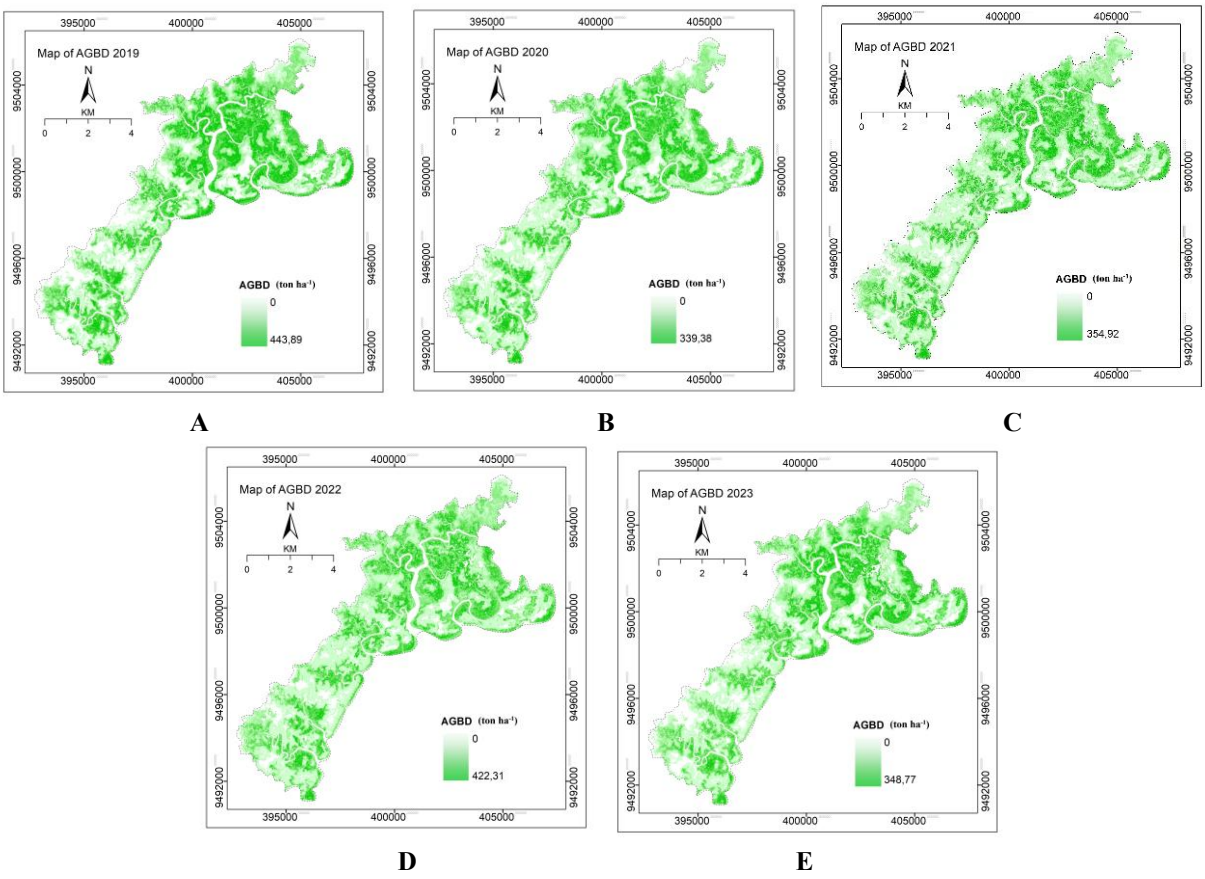

Figure 9. Distribution map of AGB (2019-2023). A. 2019, B. 2020, C. 2021, D. 2022, E. 2023

The spatial distribution maps of mangrove AGB produced from this study are important information that can be used to support REDD+ implementation and blue carbon accounting (Ahmed and Glaser 2016). The model developed in this study can help quantify carbon stocks and their temporal dynamics, which technically provide information on emission reductions and verify results-based payments (Ma 2023). In addition, the ability to capture biomass variations will improve the assessment of mangrove ecosystem services and support the design of site-specific interventions for mangrove restoration efforts and coastal resilience planning. This aligns with Harris et al. (2021), who emphasize that spatially explicit maps of forest carbon dynamics can improve transparency in emission accounting and support national climate mitigation targets, especially in tropical countries like Indonesia. The results of this study demonstrate that locally scaled research can provide valuable insights that can be applied to mangrove ecosystems in other locations with similar characteristics. A site-based approach enables the development of more context-specific conservation strategies while simultaneously contributing to the enrichment of the global knowledge base for sustainable mangrove ecosystem management.

In conclusion, this study showed that combining GEDI, Sentinel-1, Sentinel-2, and field data using machine learning methods improved the accuracy and effectiveness of mangrove forest AGB estimation in RAWNP. RF performed best among the four machine learning algorithms used to build the mangrove AGB model. Multi-season analysis from 2019 to 2023 showed that mangrove AGB in RAWNP has fluctuated. The highest occurred in 2021 and then experienced a downward trend, with the lowest observed in 2023. Areas on the edge tend to experience a decrease in AGB compared to those in the middle. Mangrove forest edges close to human activities can cause a decline in AGB. The fluctuations of AGB during 2019 – 2023 indicate the importance of appropriate management strategies to maintain the sustainability of mangrove forest functions in RAWNP. The results of this study also show that the modeling approach used has the potential to monitor mangrove biomass in real time, especially in supporting climate mitigation policies and REDD+ verification at the national level. Further studies should be directed to optimize the model parameters, integrate additional features, and investigate advanced algorithms to improve the accuracy of the resulting prediction model.

ACKNOWLEDGEMENTS

The authors are grateful to the Rawa Aopa Watumohai National Park (RAWNP) Authority, Indonesia, for the administrative support and permission to conduct this study. The authors are also grateful to Alan Saputra, Bahnur Salimin, Muhammad Ikhsan Fajrin, Aswin Anas,

and the TTM Community for their assistance in surveying and collecting field data. This study was funded by the BBPDN scholarship of the Directorate General of Higher Education, Research, and Technology, Ministry of Education and Culture of Indonesia.

REFERENCES

Ahmed N, Glaser M. 2016. Coastal aquaculture, mangrove deforestation and blue carbon emissions: is REDD+ a solution? Mar Policy 66: 58-66. DOI: 10.1016/j.marpol.2016.01.011.

Alongi DM. 2020. Global significance of mangrove blue carbon in climate change mitigation. Sci 2 (3): 67. DOI: 10.3390/sci2030067.

Alvarez E, Duque A, Saldarriaga J, Cabrera K, de las Salas G, del Valle I, Lema A, Moreno F, Orrego S, Rodríguez L. 2012. Tree above-ground biomass allometries for carbon stocks estimation in the natural forests of Colombia. For Ecol Manag 267: 297-308. DOI: 10.1016/j.foreco.2011.12.013.

Argamosa RJL, Blanco AC, Baloloy AB, Candido CG, Dumalag JBLC, Dimapilis LLC, Paringit EC. 2018. Modelling above-ground biomass of mangrove forest using Sentinel-1 imagery. ISPRS Ann Photogramm Remote Sens Spat Inf Sci IV 3 (3): 13-20. DOI: 10.5194/isprs-annals-IV-3-13-2018.

Arifanti VB, Kauffman JB, Subarno JB, Ilman M, Tosiani A, Novita N. 2022. Contributions of mangrove conservation and restoration to climate change mitigation in Indonesia. Glob Chang Biol 28 (15): 4523-4538. DOI: 10.1111/gcb.16216.

Askar, Nuthammachot N, Phairuang W, Wicaksono P, Sayektiningsih T. 2018. Estimating above-ground biomass on private forest using Sentinel-2 imagery. J Sens 2018: 6745629. DOI: 10.1155/2018/6745629.

Bai J, Meng Y, Gou R, Lyu J, Dai Z, Diao X, Zhang H, Luo Y, Zhu X, Lin G. 2021. Mangrove diversity enhances plant biomass production and carbon storage in Hainan Island, China. Funct Ecol 35 (3): 774-786. DOI: 10.1111/1365-2435.13753.

Bao HD, Huong NTT. 2025. Estimating forest above ground biomass in Dak Lak Province, Vietnam. Asian J For 9 (1): 115-123. DOI: 10.13057/asianjfor/r090112.

Bezerra E, Mafalda S, Alvarez AB, Uman-Flores DA, Perez-Torres WI, Palomino-Quispe F. 2023. A cloud coverage image reconstruction approach for remote sensing of temperature and vegetation in Amazon rainforest. Appl Sci 13 (23): 12900. DOI: 10.3390/app132312900.

Bruening JM, Fischer R, Bohn FJ, Armston J, Armstrong AH, Knapp N, Tang H, Huth A, Dubayah R. 2021. Challenges to above-ground biomass prediction from waveform LiDAR. Environ Res Lett 16 (12): 125013. DOI: 10.1088/1748-9326/ac3cec.

Bryan-Brown DN, Connolly RM, Richards DR, Adame F, Friess DA, Brown CJ. 2020. Global trends in mangrove forest fragmentation. Sci Rep 10 (1): 7117. DOI: 10.1038/s41598-020-63880-1.

Budiman F. 2019. SVM-RBF parameters testing optimization using cross validation and grid search to improve multiclass classification. Sci Vis 11 (1): 80-90. DOI: 10.26583/sv.11.1.07.

Budiman I, Mubarak A, Kapita S, Abdullah SD, Salmin M. 2021. Implementation of backpropagation artificial network methods for early children's intelligence prediction. E3S Web Conf 328 04033. DOI: 10.1051/e3sconf/202132804033.

Bullock EL, Healey SP, Yang Z, Acosta R, Villalba H, Insfrán KP, Melo JB, Wilson S, Duncanson L, Næsset E, Armston J, Saarela S, Ståhl G, Patterson PL, Dubayah R. 2023. Estimating above-ground biomass density using hybrid statistical inference with GEDI LiDAR data and Paraguay's National Forest Inventory. Environ Res Lett 18 (8): 085001. DOI: 10.1088/1748-9326/acdf03.

Bunting P, Rosenqvist A, Hilarides L, Lucas RM, Thomas N, Tadono T, Worthington TA, Spalding M, Murray NJ, Rebelo LM. 2022. Global mangrove extent change 1996-2020: Global mangrove. Remote Sens 14 (15): 3657. DOI: 10.3390/rs14153657.

Cameron C, Hutley LB, Friess DA, Brown B. 2019. Community structure dynamics and carbon stock change of rehabilitated mangrove forests in Sulawesi, Indonesia. Ecol Appl 29 (1): e01810. DOI: 10.1002/eap.1810.

Carugati L, Gatto B, Rastelli E, Lo Martire M, Coral C, Greco S, Danovaro R. 2018. Impact of mangrove forests degradation on biodiversity and ecosystem functioning. Sci Rep 8 (1): 13298. DOI: 10.1038/s41598-018-31683-0.

Chave J, Andalo C, Brown S, Cairns MA, Chambers JQ, Eamus D, Fölster H, Fromard F, Higuchi N, Kira T, Lescure JP, Nelson BW, Ogawa H, Puig H, Riéra B, Yamakura T. 2005. Tree allometry and improved estimation of carbon stocks and balance in tropical forests. Oecologia 145 (1): 87-99. DOI: 10.1007/s00442-005-0100-x.

Chen S, Useya J, Mugiyo H. 2020. Decision-level fusion of Sentinel-1 SAR and Landsat 8 OLI texture features for crop discrimination and classification: Case of Masvingo, Zimbabwe. Heliyon 6 (11): e05358. DOI: 10.1016/j.heliyon.2020.e05358.

Coetzee C. 2022. Change detection of vegetation cover using remote sensing and GIS – a case study of the West Coast Region of South Africa. Geogr Environ Sustain 15 (2): 91-102. DOI: 10.24057/2071-9388-2021-067.

Devaney JL, Marone D, McElwain JC. 2021. Impact of soil salinity on mangrove restoration in a semiarid region: A case study from the Saloum Delta, Senegal. Restor Ecol 29 (2): e13186. DOI: 10.1111/rec.13186.

Dubayah R, Blair JB, Goetz S, Fatoyinbo L, Hansen M, Healey S, Hofton M, Hurtt G, Kellner J, Luthcke S, Armston J, Tang H, Duncanson L, Hancock S, Jantz P, Marselis S, Patterson PL, Qi W, Silva C. 2020. The global ecosystem dynamics investigation: High-resolution laser ranging of the Earth's forests and topography. Sci Remote Sens 1: 100002. DOI: 10.1016/j.srs.2020.100002.

Goodbody TRH, Coops NC, Queinnec M, White JC, Tompalski P, Hudak AT, Auty D, Valbuena R, LeBoeuf A, Sinclair I, McCartney G, Prieur J, Woods ME. 2023. sgsR : A structurally guided sampling toolbox for LiDAR-based forest inventories. Forestry 96 (4): 411-424. DOI: 10.1093/forestry/cpac055.

Gouvêa LP, Serrão EA, Cavanaugh K, Gurgel CFD, Horta PA, Assis J. 2022. Global impacts of projected climate changes on the extent and above-ground biomass of mangrove forests. Divers Distrib 28 (11): 2349-2360. DOI: 10.1111/ddi.13631.

Gu Z, Cao M, Wang C, Yu N, Qing H. 2022. Research on mining maximum subsidence prediction based on genetic algorithm combined with XGBoost model. Sustainability 14 (16): 10421. DOI: 10.3390/su141610421.

Gupta R, Sharma LK. 2022. Above-ground biomass prediction by fusing GEDI footprints with optical and SAR data using the Random Forest in the mixed tropical forest, India. IEEE Intl Geosci Remote Sens Symp 2022: 5460-5463. DOI: 10.1109/IGARSS46834.2022.9883443.

Habibullah I, Sanjaya H, Putra ING. 2023. Utilization of the indices to detect and monitor the landcover changes of mangroves. IOP Conf Ser: Earth Environ Sci 1127 (1): 012033. DOI: 10.1088/1755-1315/1127/1/012033.

Hamuna B, Kalor JD, Tablaseray VE. 2019. The impact of tsunami on mangrove spatial change in eastern coastal of Biak Island, Indonesia. J Ecol Eng 20 (3): 1-6. DOI: 10.12911/22998993/95094.

Harris NL, Gibbs DA, Baccini A, Birdsey RA, de Bruin S, Farina M, Fatoyinbo L, Hansen MC, Herold M, Houghton RA, Potapov PV, Suarez DR, Roman-Cuesta RM, Saatchi SS, Slay CM, Turubanova SA, Tyukavina A. 2021. Global maps of twenty-first century forest carbon fluxes. Nat Clim Chang 11 (3): 234-240. DOI: 10.1038/s41558-020-00976-6.

Hernández-Stefanoni JL, Castillo-Santiago MÁ, Mas JF, Wheeler CE, Andres-Mauricio J, Tun-Dzul F, George-Chacón SP, Reyes-Palomeque G, Castellanos-Basto B, Vaca R, Dupuy JM. 2020. Improving above-ground biomass maps of tropical dry forests by integrating LiDAR, ALOS PALSAR, climate and field data. Carbon Balance Manag 15 (1): 15. DOI: 10.1186/s13021-020-00151-6.

Hickey SM, Radford B. 2022. Turning the tide on mapping marginal mangroves with multi-dimensional space–time remote sensing. Remote Sens 14 (14): 3365. DOI: 10.3390/rs14143365.

Hidayah Z, Utama RYS, As-Syakur AR, Rachman HA, Wiyanto DB. 2024. Mapping mangrove above-ground carbon stock of Benoa Bay, Bali using Sentinel-1 satellite imagery. IOP Conf Ser: Earth Environ Sci 1298 (1): 012013. DOI: 10.1088/1755-1315/1298/1/012013.

Hu H, Zhou H, Cao K, Lou W, Zhang G, Gu Q, Wang J. 2024. Biomass estimation of milk vetch using UAV hyperspectral imagery and machine learning. Remote Sens 16 (12): 2183. DOI: 10.3390/rs16122183.

Hu T, Zhang YY, Su Y, Zheng Y, Lin G, Guo Q. 2020. Mapping the global mangrove forest above-ground biomass using multi-source

remote sensing data. Remote Sens 12 (10): 1690. DOI: 10.3390/rs12101690.

Huang AT, Gillett ZE, Taschetto AS. 2024. Australian rainfall increases during multi-year La Niña. Geophys Res Lett 51 (9): e2023GL106939. DOI: 10.1029/2023GL106939.

Indrayani E, Kalor JD, Warpur M, Hamuna B. 2021. Using allometric equations to estimate mangrove biomass and carbon stock in Demta Bay, Papua Province, Indonesia. J Ecol Eng 22 (5): 263-271. DOI: 10.12911/22998993/135945.

İspir DA. 2025. Spatiotemporal monitoring of the surface water level dynamics in Lake Tuz, Türkiye, using remote sensing and GIS. DYSONA: Appl Sci 6: 387-388. DOI: 10.30493/das.2025.506287.

Jantol N, Prikaziuk E, Celesti M, Hernandez-Sequeira I, Tomelleri E, Pacheco-Labrador J, Van Wittenberghe S, Pla F, Bandopadhyay S, Koren G, Siegmann B, Legović T, Kutnjak H, Cendrero-Mateo MP. 2023. Using Sentinel-2-based metrics to characterize the spatial heterogeneity of FLEX sun-induced chlorophyll fluorescence on sub-pixel scale. Remote Sens 15 (19): 4835. DOI: 10.3390/rs15194835.

Kacic P, Hirner A, Da Ponte E. 2021. Fusing Sentinel-1 and-2 to model GEDI-derived vegetation structure characteristics in GEE for the Paraguayan Chaco. Remote Sens 13 (24): 5105. DOI: 10.3390/rs13245105.

Kumar L, Mutanga O. 2018. Google Earth Engine applications since inception: Usage, trends, and potential. Remote Sens 10 (10): 1509. DOI: 10.3390/rs10101509.

Labriere N, Tao S, Chave J et al. 2018. In situ reference datasets from the TropiSAR and AfriSAR campaigns in support of upcoming spaceborne biomass missions. IEEE J Sel Top Appl Earth Observ Remote Sens 11 (10): 3617-3627. DOI: 10.1109/JSTARS.2018.2851606.

Lang N, Kalischek N, Armston J, Schindler K, Dubayah R, Wegner JD. 2022. Global canopy height regression and uncertainty estimation from GEDI LiDAR waveforms with deep ensembles. Remote Sens Environ 268 (October 2021), 112760. DOI: 10.1016/j.rse.2021.112760.

Liu A, Cheng X, Chen Z. 2021. Performance evaluation of GEDI and ICESat-2 laser altimeter data for terrain and canopy height retrievals. Remote Sens Environ 264: 112571. DOI: 10.1016/j.rse.2021.112571.

Liu C, Chen D, Zou C, Liu S, Li H, Liu Z, Feng W, Zhang N, Ye L. 2022. Modeling biomass for natural subtropical secondary forest using multi-source data and different regression models in Huangfu Mountain, China. Sustainability 14 (20): 13006. DOI: 10.3390/su142013006.

London AJ. 2019. Artificial intelligence and black-box medical decisions: Accuracy versus explainability. Hastings Cent Rep 49 (1): 15-21. DOI: 10.1002/hast.973.

López-Serrano PM, Domínguez JLC, Corral-Rivas JJ, Jiménez E, López-Sánchez CA, Vega-Nieva DJ. 2020. Modeling of above-ground biomass with Landsat 8 OLI and machine learning in temperate forests. Forests 11 (1); 11. DOI: 10.3390/f11010011.

Luo Y, Yan L, Zhou Z, Huang D, Cai L, Du S, Yang Y, Huang Y, Li Q. 2024. Estimation of the above-ground biomass of forests in complex mountainous areas using regression kriging. Forests 15 (10): 1734. DOI: 10.3390/f15101734.

Lutz N, Rodriguez-Veiga P, Oliveras Menor I. 2024. Estimating vegetation structure and above-ground carbon storage in Western Australia using GEDI LiDAR, Landsat and Sentinel data. Environ Res Ecol 3 (4): 045004. DOI: 10.1088/2752-664X/ad7f5a.

Ma W. 2023. A comparative study of carbon pricing policies in China and the Scandinavian countries: Lessons for effective climate change mitigation with a focus on Sweden. E3S Web Conf 424: 04005. DOI: 10.1051/e3sconf/202342404005.

Manley W, Tran T, Prusinski M, Brisson D. 2023. Modeling tick populations: An ecological test case for gradient boosted trees. Peer Community J 3: e116. DOI: 10.24072/pcjournal.353.

Marselis SM, Abernethy K, Alonso A et al. 2020. Evaluating the potential of full-waveform LIDAR for mapping pan-tropical tree species richness. Glob Ecol Biogeogr 29 (10): 1799-1816. DOI: 10.1111/geb.13158.

Masiello G, Ripullone F, De Feis I, Rita A, Saulino L, Pasquariello P, Cersosimo A, Venafra S, Serio C. 2022. The IASI water deficit index to monitor vegetation stress and early drying in summer heatwaves: An application to southern Italy. Land 11 (8): 1336. DOI: 10.3390/land11081366.

Matto AA, Jaikishun S, Ram M. 2023. Impacts of different salinity levels on seedling growth and survival of black mangrove (Avicennia germinans). Asian J For 7 (1): 67-73. DOI: 10.13057/asianjfor/r070108.

Maureaud A, Hodapp D, Van Denderen PD, Hillebrand H, Gislason H, Spaanheden Dencker T, Beukhof E, Lindegren M. 2019. Biodiversity–ecosystem functioning relationships in fish communities: biomass is related to evenness and the environment, not to species richness. Proc R Soc B 286 (1906): 20191189. DOI: 10.1098/rspb.2019.1189.

Mills-Novoa M, Liverman DM. 2019. Nationally determined contributions: Material climate commitments and discursive positioning in the NDCs. WIREs Clim Chang 10 (5): e589. DOI: 10.1002/wcc.589.

Moradi F, Zarei A, Ranjbar S, Homayouni S. 2023. Wheat biomass estimation from UAV imagery using an ensemble learning approach with Bayesian optimization. ISPRS Ann Photogramm Remote Sens Spat Inf Sci 10 (4/W1-2022): 515-522. DOI: 10.5194/isprs-annals-X-4-W1-2022-515-2023.

Mosfeldt M, Jørgensen HL, Lauritzen JB, Jansson KÅ. 2024. Development and internal validation of a multivariable prediction model for mortality after hip fracture with machine learning techniques. Calcif Tissue Intl 114 (6): 568-582. DOI: 10.1007/s00223-024-01208-1.

Moudrý V, Prošek J, Marselis S, Marešová J, Šárovcová E, Gdulová K, Kozhoridze G, Torresani M, Rocchini D, Eltner A, Liu X, Potůčková M, Šedová A, Crespo-Peremarch P, Torralba J, Ruiz LA, Perrone M, Špatenková O, Wild J. 2024. How to find accurate terrain and canopy height GEDI footprints in temperate forests and grasslands? Earth Space Sci 11 (10): e2024EA003709. DOI: 10.1029/2024EA003709.

Munthe CR, Sulistiyono N. 2023. Above ground carbon estimation using Sentinel-1B radar satellite imagery. J Phys: Conf Ser 2421 (1): 01237. DOI: 10.1088/1742-6596/2421/1/012037.

Nandy S, Srinet R, Padalia H. 2021. Mapping forest height and above-ground biomass by integrating ICESat-2, Sentinel-1 and Sentinel-2 data using random forest algorithm in northwest Himalayan Foothills of India. Geophys Res Lett 48 (14): e2021GL093799. DOI: 10.1029/2021GL093799.

Narvaes IDS, Santos JRD, Bispo PDC, Graça PMDA, Guimarães US, Gama FF. 2023. Estimating forest above-ground biomass in Central Amazonia using polarimetric attributes of ALOS/PALSAR images. Forests 14 (5): 941. DOI: 10.3390/f14050941.

Ni W, Zhang Z, Sun G. 2021. Assessment of slope-adaptive metrics of GEDI waveforms for estimations of forest above-ground biomass over mountainous areas. J Remote Sens 2021: 9805364. DOI: 10.34133/2021/9805364.

Nur AAI, Arifiani KN, Ramadhandi AR, Sabrina AD, Nugroho GD, Kusumaningrum L, Ramdhun D, Bao TQ, Yap CK, Budiharta S, Setyawan AD. 2022. Estimation of above-ground biomass and carbon stock in Damas Beach, Trenggalek District, East Java, Indonesia. Indo Pac J Ocean Life 6 (2): 80-86. DOI: 10.13057/oceanlife/o060203.

Oehmcke S, Li L, Revenga JC, Nord-Larsen T, Trepekli K, Gieseke F, Igel C. 2022. Deep learning based 3D point cloud rregression for estimating forest biomass. GIS: Proc ACM Intl Symp Adv Geogr Inf Syst 38: 1-4. DOI: 10.1145/3557915.3561471.

Otero V, Lucas R, Van De Kerchove R, Satyanarayana B, Mohd-Lokman H, Dahdouh-Guebas F. 2020. Spatial analysis of early mangrove regeneration in the Matang Mangrove Forest Reserve, Peninsular Malaysia, using geomatics. For Ecol Manag 472: 118213. DOI: 10.1016/j.foreco.2020.118213.

Othman AAA, Tariq Z, Aljawad MS, Yan B, Kamal MS. 2023. Enhancing fracturing fluid viscosity in high salinity water: A data-driven approach for prediction and optimization. Energy Fuels 37 (17): 13065-13079. DOI: 10.1021/acs.energyfuels.3c02272.

Pena-Regueiro J, Sebastiá-Frasquet MT, Estornell J, Aguilar-Maldonado JA. 2020. Sentinel-2 application to the surface characterization of small water bodies in wetlands. Water 12 (5): 1487. DOI: 10.3390/w12051487.

Pham TD, Yokoya N, Bui DT, Yoshino K, Friess DA. 2019. Remote sensing approaches for monitoring mangrove species, structure, and biomass: Opportunities and challenges. Remote Sens 11 (3): 230. DOI: 10.3390/rs11030230.

Picard N, Fonton N, Bosela FB, Fayolle A, Loumeto J, Ayecaba GN, Sonké B, Diane O, Bombo Y, Maïdou HM, Ngomanda A. 2025. Selecting allometric equations to estimate forest biomass from plot- rather than individual-level predictive performance, Biogeosciences 22: 1413-1426, DOI: 10.5194/bg-22-1413-2025.

Ploton P, Mortier F, Réjou-Méchain M, Barbier N, Picard N, Rossi V, Dormann C, Cornu G, Viennois G, Bayol N, Lyapustin A, Gourlet-Fleury S, Pélissier R. 2020. Spatial validation reveals poor predictive performance of large-scale ecological mapping models. Nat Commun 11 (1): 4540. DOI: 10.1038/s41467-020-18321-y.

Qian L, Xuan L, Chen J. 2023. Battery SOH estimation based on decision tree and improved support vector machine regression algorithm. Front Energy Res 11: 1218580. DOI: 10.3389/fenrg.2023.1218580.

Qiptiyah M, Broto BW, Setiawan H. 2013. Keragaman jenis burung pada kawasan mangrove di Taman Nasional Rawa Aopa Watumohai. Jurnal Penelitian Kehutanan Wallacea 2 (1): 41-50. DOI: 10.18330/jwallacea.2013.vol2iss1pp41-50.

Rengarajan R, Schott JR. 2018. Evaluation of sensor and environmental factors impacting the use of multiple sensor data for time-series applications. Remote Sens 10 (11): 1678. DOI: 10.3390/rs10111678.

Ridha MA, Kusrini MD, Mardiastuti A, Karraker N. 2021. The amphibians and reptiles of Rawa Aopa Watumohai National Park, Southeast Sulawesi. Media Konservasi 26 (2): 128-138. DOI: 10.29244/medkon.26.2.128-138.

Rijal SS, Pham TD, Noer'Aulia S, Putera MI, Saintilan N. 2023. Mapping mangrove above-ground carbon using multi-source remote sensing data and machine learning approach in Loh Buaya, Komodo National Park, Indonesia. Forests 14 (1): 94. DOI: 10.3390/f14010094.

Rishmawi K, Huang C, Schleeweis K, Zhan X. 2022. Integration of VIIRS observations with GEDI-LIDAR measurements to monitor forest structure dynamics from 2013 to 2020 across the conterminous United States. Remote Sens 14 (10): 2320. DOI: 10.3390/rs14102320.

Rocha SJSSD, Romero FMB, Torres CMME, Jacovine LAG, Ribeiro SC, Villanova PH, Schettini BLS, Junior VTMDM, Reis LP, Rufino MPMX, Comini IB, Tavares Júnior IDS, Viana ÁBT. 2023. Machine learning: Volume and biomass estimates of commercial trees in the Amazon forest. Sustainability 15 (12): 9452. DOI: 10.3390/su15129452.

Rondon M, Ewane EB, Abdullah MM et al. 2023. Remote sensing-based assessment of mangrove ecosystems in the gulf cooperation council countries: A systematic review. Front Mar Sci 10: 1241928. DOI: 10.3389/fmars.2023.1241928.

Roozbeh M, Rouhi A, Mohamed NA, Jahadi F. 2023. Generalized support vector regression and symmetry functional regression approaches to model the high-dimensional data. Symmetry 15 (6): 1262. DOI: 10.3390/sym15061262.

Rudianto R, Bengen DG, Kurniawan F. 2020. Causes and effects of mangrove ecosystem damage on carbon stocks and absorption in East Java, Indonesia. Sustainability 12 (24): 10319. DOI: 10.3390/su122410319.

Saldaña-Villota TM, Cotes-Torres JM. 2021. Comparison of statistical indices for the evaluation of crop models performance. Revista Facultad Nacional de Agronomia Medellin 74 (3): 9675-9684. DOI: 10.15446/rfnam.v74n3.93562.

Sasmito SD, Taillardat P, Clendenning JN, Cameron C, Friess DA, Murdiyarso D, Hutley LB. 2019. Effect of land-use and land-cover change on mangrove blue carbon: A systematic review. Glob Chang Biol 25 (12): 4291-4302. DOI: 10.1111/gcb.14774.

Shi Y, Wang Z, Zhang G, Wei X, Ma W, Yu H. 2024. Evaluating the research status of the remote sensing-mediated monitoring of forest biomass: A bibliometric analysis of WOS. Forests 15 (3): 524. DOI: 10.3390/f15030524.

Simard M, Fatoyinbo L, Smetanka C, Rivera-Monroy VH, Castañeda-Moya E, Thomas N, Van der Stocken T. 2019. Mangrove canopy height globally related to precipitation, temperature and cyclone frequency. Nat Geosci 12 (1): 40-45. DOI: 10.1038/s41561-018-0279-1.

Sparks AM, Corrao MV, Keefe RF, Armstrong R, Smith AMS. 2024. An accuracy assessment of field and airborne laser scanning–derived individual tree inventories using felled tree measurements and log scaling data in a mixed conifer forest. For Sci 70 (3): 228-241. DOI: 10.1093/forsci/fxae015.

Stoffel MA, Nakagawa S, Schielzeth H. 2021. partR2: Partitioning R2 in generalized linear mixed models. PeerJ 9: e11414. DOI: 10.7717/peerj.11414.

Sudirman N, Salim HL, Rustam A, Ati RNA, Hernina R, Marini Y, Suryono DD. 2023. Assessment of mangrove ecosystem potential in Bontang Regency-East Kalimantan to reduce abrasion. IOP Conf Ser: Earth Environ Sci 1148 (1): 012041. DOI: 10.1088/1755-1315/1148/1/012041.

Suwanto A, Takarina ND, Koestoer RH, Frimawaty E. 2021. Diversity, biomass, covers, and NDVI of restored mangrove forests in Karawang and Subang coasts, West Java, Indonesia. Biodiversitas 22 (9): 4115-4122. DOI: 10.13057/biodiv/d220960.

Suyarso, Avianto P. 2022. AMMI Automatic Mangrove Map and Index: Novelty for efficiently monitoring mangrove changes with the case study in Musi Delta, South Sumatra, Indonesia. Intl J For Res 2022 (1): 8103242. DOI: 10.1155/2022/8103242.

Tamga DK, Latifi H, Ullmann T, Baumhauer R, Bayala J, Thiel M. 2023. Estimation of above-ground biomass in agroforestry systems over three climatic regions in West Africa using Sentinel-1, Sentinel-2, ALOS, and GEDI data. Sensors 23 (1): 349. DOI: 10.3390/s23010349.

Tavasoli N, Arefi H. 2021. Comparison of capability of SAR and optical data in mapping forest above ground biomass based on machine learning. Environ Sci Proc 5 (1): 13. DOI: 10.3390/iecg2020-07916.

Tian X, Li J, Zhang F, Zhang H, Jiang M. 2024. Forest above-ground biomass estimation using multi-source remote sensing data and deep learning algorithms: A case study over Hangzhou Area in China. Remote Sens 16 (6): 1074. DOI: 10.3390/rs16061074.

Utami W, Sugiyanto C, Rahardjo N. 2024a. Analysing the driving forces of carbon stock change for climate change mitigation. Ecol Eng Environ Technol 25 (11): 83-101. DOI: 10.12912/27197050/192222.

Utami W, Sugiyanto C, Rahardjo N. 2024b. Mangrove area degradation and management strategies in Indonesia: A review. J Degrad Min Lands Manag 11 (3): 6037-6047. DOI: 10.15243/jdmlm.2024.113.6037.

Wang G, Li S, Huang C, He G, Li Y, Feng J, Tang F, Yan P, Qiu L. 2023. Mapping the spatial distribution of above-ground biomass in China's subtropical forests based on UAV LiDAR data. Forests 14 (8): 1560. DOI: 10.3390/f14081560.

Wang W. 2024. Forecasting the population of China from 2020 to 2025 based on random forest and linear regression. Highlights Sci Eng Technol 85: 511-518. DOI: 10.54097/a70zsh28.

Winanti WS, Sudinda TW, Oktivia R, Ihsan IM, Ikhwanuddin M, Amru K, Anjani R, Aryantie MH. 2023. Barrier analysis to leverage the climate change mitigation-adaptation implementation action in mangrove forest and its surrounding community villages. IOP Conf Ser: Earth Environ Sci 1201 (1): 012062. DOI: 10.1088/1755-1315/1201/1/012062.

Wu L, Huang R, Tetko IV, Xia Z, Xu J, Tong W. 2021. Trade-off predictivity and explainability for machine-learning powered predictive toxicology: An in-depth investigation with Tox21 data sets. Chem Res Toxicol 34 (2): 541-549. DOI: 10.1021/acs.chemrestox.0c00373.

Xiao J, Chen L, Zhang T, Li L, Yu Z, Wu R, Bai L, Xiao J, Chen L. 2022. Identification of urban green space types and estimation of above-ground biomass using Sentinel-1 and Sentinel-2 data. Forests 13 (7): 1077. DOI: 10.3390/f13071077.

Xu K, Xu Y, Ye Y, Chen W. 2022. Novel feature selection method for nonlinear support vector regression. Complexity 2022: 4740173. DOI: 10.1155/2022/4740173.

Yates LA, Aandahl Z, Richards SA, Brook BW. 2023. Cross validation for model selection: A review with examples from ecology. Ecol Monogr 93 (1): e1557. DOI: 10.1002/ecm.1557.

Yu T, Zhang Q, Sun R. 2021. Spatial representativeness of gross primary productivity from carbon flux sites in the Heihe River Basin, China. Remote Sens 13 (24): 5016. DOI: 10.3390/rs13245016.

Zanne AE, Lopez-Gonzalez G, Coomes DA, Ilic J, Jansen S, Lewis SL, Miller RB, Swenson NG, Wiemann MC, Chave J. 2009. Data from: Towards a Worldwide Wood Economics Spectrum [Dataset]. Dryad. DOI: 10.5061/dryad.234.

Zarco-Tejada PJ, Hornero A, Beck PSA, Kattenborn T, Kempeneers P, Hernández-Clemente R. 2019. Chlorophyll content estimation in an open-canopy conifer forest with Sentinel-2A and hyperspectral imagery in the context of forest decline. Remote Sens Environ 223: 320-335. DOI: 10.1016/j.rse.2019.01.031.

Zhang Q, Xu L, Zhang M, Wang Z, Gu Z, Wu Y, Shi Y, Lu Z. 2020. Uncertainty analysis of remote sensing pretreatment for biomass estimation on Landsat OLI and Landsat ETM+. ISPRS Intl J Geo-Inf 9 (1): 48. DOI: 10.3390/ijgi9010048.

Zhou Y, Taylor DM, Tang H. 2025. Improved country-wide estimation of above-ground tropical forest biomass using locally calibrated GEDI spaceborne LiDAR data. Environ Res Lett 20 (1): 014017. DOI: 10.1088/1748-9326/ad9aba.